Neointima and neoatherosclerotic characteristics in bare metal and first- and second-generation drug-eluting stents in patients admitted with cardiovascular events attributed to stent failure: an optical coherence tomography study

Rodrigue Stettler[1], MD; Jouke Dijkstra[2], PhD; Lorenz Räber[3], MD, PhD; Ryo Torii[4], PhD; Yao-Jun Zhang[5], MD, PhD; Antonis Karanasos[6], MD, PhD; Shengnan Liu[2], MSc; Tom Crake[1], MD; Steve Hamshere[1], MBBS; Hector M. Garcia-Garcia[6], MD, PhD; Erhan Tenekecioglu[6], MD, PhD; Muhiddin Ozkor[1], MD; Stephan Windecker[3], MD; Patrick W. Serruys[6,7], MD, PhD; Evelyn Regar[6], MD, PhD; Anthony Mathur[1], MD, PhD; Christos V. Bourantas[1,8]*, MD, PhD

1. Barts Heart Centre, Barts Health NHS Trust, London, United Kingdom; 2. Leiden University Medical Centre, Leiden, the Netherlands; 3. Department of Cardiology, Bern University Hospital, Bern, Switzerland; 4. Department of Mechanical Engineering, University College London, London, United Kingdom; 5. Nanjing First Hospital, Nanjing Medical University, Nanjing, China; 6. Thoraxcenter, Erasmus Medical Center, Rotterdam, the Netherlands; 7. Faculty of Medicine, National Heart & Lung Institute, Imperial College London, London, United Kingdom; 8. Institute of Cardiovascular Sciences, University College London, London, United Kingdom

GUEST EDITOR: Peter Barlis, MBBS, MPH, PhD; Melbourne Medical School, University of Melbourne, Melbourne, Victoria, Australia

Abstract

Aims: The aim of this study was to assess neoatherosclerotic plaque morphology in bare metal (BMS) and first- and second-generation drug-eluting stents (DES) in patients presenting with an event attributed to stent failure.

Methods and results: Thirty-five patients (11 implanted with BMS, 13 with a first-generation and 11 with a second-generation DES) admitted with an event due to stent failure who had neoatherosclerotic lesions on optical coherence tomography were included in the analysis. The lumen and stent borders were detected and the lipid and calcific tissue were identified in the neointima and their burden was estimated. The neointima attenuation and backscatter indices were computed and compared between the different stent types. Although there were no differences in the neointima burden, the BMS group exhibited thinner fibrous caps (p<0.001), and a numerically increased incidence of lipid-rich plaques (p=0.052) and macrophage accumulation (p=0.012). Neointima discontinuities (p=0.009) and thrombus (p=0.032) were seen more often in first-generation DES. In all stent types, neoatherosclerosis had focal manifestations. In neoatherosclerotic lesions the attenuation and backscatter indices were increased in BMS (p=0.031 and p=0.018, respectively) compared to DES; however, there were no differences between stents in the attenuation indices in subsegments located distally to neoatherosclerotic lesions which had low values in all stent types.

Conclusions: Although there are differences in lipid burden and neointima characteristics in different stent types, in all stents neoatherosclerosis has focal manifestations indicating that, irrespective of the stent type, focal triggers are involved in the generation of vulnerable neolesions.

*Corresponding author: Barts Heart Centre, 1 St Martin's Le Grand, London, EC1A 7BE, United Kingdom.
E-mail: Christos.Bourantas@bartshealth.nhs.uk

Abbreviations

BMS   bare metal stent
DES   drug-eluting stent
OCT   optical coherence tomography
TCFA thin-cap fibroatheroma

Introduction

Neoatherosclerosis, i.e., the development of high-risk lesions within stented segments, has been increasingly recognised as a common cause of late stent failure. Histology studies have shown that the incidence of neoatherosclerosis increases with time and appears earlier in first-generation than in second-generation drug-eluting stents (DES) or bare metal stents (BMS)[1]. Optical coherence tomography (OCT) appears able to assess neoatherosclerotic lesion characteristics and today it is the preferable modality for the *in vivo* detection of neoatherosclerosis. OCT has been extensively used in recent years to assess the prevalence of neoatherosclerotic lesions in different stent types[2-4] and patient populations[5], and has allowed identification of predictors[6] associated with the development of neoatherosclerotic plaques. However, there are limited data about neoatherosclerotic characteristics and neointima morphology in different stent types in patients admitted with a neoatherosclerotic-related cardiovascular event[2].

Methods

Five experts (R. Stettler, L. Räber, A. Karanasos, Y. Zhang, C. Bourantas) reviewed the OCT data in four hospitals (Barts Health NHS Trust, London, UK; Bern University Hospital, Bern, Switzerland; Nanjing First Hospital, Nanjing, China and Thoraxcenter, Erasmus MC, Amsterdam, the Netherlands, respectively) and identified consecutive patients with neoatherosclerotic lesions admitted with a cardiovascular event attributed either to stent restenosis or to neoatherosclerotic plaque rupture. The inclusion criteria were: 1) patients admitted with an acute coronary syndrome (defined as ST-elevation or non-ST-elevation myocardial infarction) or stable angina attributed to stent restenosis or neoatherosclerotic plaque rupture, 2) assessment of the culprit stented segment with Fourier domain OCT before balloon predilation, and 3) presence of neoatherosclerotic lesions in the stented segment. Exclusion criteria included: 1) poor quality OCT imaging, extensive thrombus or lipid burden that did not allow visualisation of the lumen and stent circumference in >180° for a length >0.8 mm, 2) segments with stent overlapping >5 mm, and 3) segments implanted with different stent types (i.e., BMS and DES or first- and second-generation DES).

Sirolimus-eluting (CYPHER®; Cordis, Milpitas, CA, USA) and paclitaxel-eluting (TAXUS®; Boston Scientific, Marlborough, MA, USA) stents were classified as first-generation DES, while zotarolimus-eluting (Endeavor® Sprint or Resolute™; Medtronic, Santa Rosa, CA, USA), biolimus (BioMatrix™; Biosensors Inc, Singapore), and everolimus-eluting (XIENCE®; Abbott Vascular, Santa Clara, CA, USA) stents were classified as second-generation DES. The study was approved by the local ethics review committee of the institution that conducted the study.

OPTICAL COHERENCE TOMOGRAPHY – DATA ACQUISITION

OCT images were acquired with either a C7XR™ or an OPTIS™ (St. Jude Medical, St. Paul, MN, USA) or a LUNAWAVE® (Terumo Corp., Tokyo, Japan) system. All OCT pullbacks were performed prior to balloon predilation; segments treated with thrombus aspiration before OCT were included in the analysis. Pullback was performed at a constant speed (range: 18-40 mm/s) with the use of an automated pullback device during continuous injection of contrast medium through the guide catheter. The frame rates were 180 fr/s for the OPTIS, 100 fr/s for the C7XR and 160 fr/s for the LUNAWAVE system.

SEGMENTATION OF OPTICAL COHERENCE TOMOGRAPHIC DATA

OCT imaging analysis was performed offline using proprietary software (QCM-CMS; Leiden University Medical Center, Leiden, the Netherlands). The stented segments were identified and the OCT frames in these segments were analysed at 0.4 mm intervals (0.375 mm for the LUNAWAVE system) by two independent analysts (R. Stettler and C.V. Bourantas), blinded to stent type and patient characteristics. The lumen and the stent border were detected, and the neointima was defined as the tissue between the lumen and the endoluminal border of the struts. Neointima burden was defined as: $100 \times$ neointima area vs. stent area. Neoatherosclerosis was defined as neointima with either a lipid or a calcific tissue[7]. The border of the fibrous cap over lipid tissue was segmented using semi-automated software (QCM-CMS) and the minimum and mean cap thickness were calculated[8]. The borders of the lipid and calcific tissue were detected and the lipid area, the lipid arc, and the calcific area were estimated. The lipid/calcific burden was defined as: $100 \times$ lipid/calcific area vs. neointima area. Thin-cap fibroatheroma (TCFA) was defined as lipid tissue with a fibrous cap thickness ≤65 μm; a cap thickness >65 μm was characterised as fibroatheroma.

Neoatherosclerotic lesions were defined as calcific tissue, TCFA, or fibroatheroma in the neointima. A gap of at least 0.5 mm was used to define the boundary between two neoatherosclerotic lesions.

In addition, the two observers identified the presence of macrophages, neovessels, cholesterol crystals, thrombus and neointima discontinuities (i.e., flaps, cavities, double lumen and fissures)[9].

ATTENUATION AND BACKSCATTER ANALYSIS

In each OCT cross-section the attenuation and backscatter indices were estimated for the neointima tissue using established methodologies, by a module developed by Leiden University Medical Center (Leiden, the Netherlands)[10,11]. In contrast to previous reports, the analysis was performed in the entire circumference of the neointima[4]. In order to exclude the strut effect in each cross-section, the stent border was moved 100 μm inwards to the original border and the region of interest was defined by this curve and the lumen border. The guidewire artefact was also removed and then the 95 percentile values were estimated for each frame.

The output of this analysis was colour-coded displayed in each cross-section and in spread-out stent plots. Frames portraying lipid-rich neointima are anticipated to have a higher attenuation and backscatter indices in the inner border of the lipid tissue and low indices in the lipid tissue resulting in low mean attenuation values. Therefore, the 95 percentile attenuation and backscatter values were used to identify degenerative changes in the neointima. We compared the 95 percentile attenuation and backscatter values: 1) between different stent types, and 2) between subsegments with neoatherosclerosis, subsegments located adjacent (2 mm), and subsegments located distally (>2 mm) to neoatherosclerotic lesions. Only frames with attenuation/backscatter values for an arc >180° of the circumference of the neointima were included in the analysis. Frames with poor flushing and thrombus were also excluded.

REPRODUCIBILITY OF OCT ANALYSIS

The accuracy and reproducibility of the OCT analysis was assessed by estimating the inter- and intra-observer variability of the two analysts in six patients (424 frames). The κ test of concordance was used to assess observer agreement. A high intra- and inter-observer agreement was noted in the detection of neoatherosclerotic, lipid, calcific tissue and thrombus (κ in all cases >0.80), whereas the agreement of the observers in identifying macrophages was moderate (intra-observer variability: 0.72, inter-observer variability: 0.75).

STATISTICAL ANALYSIS

The Kolmogorov-Smirnov test was used to assess the distribution of continuous variables which are reported as mean±standard deviation when they are normally distributed, and median and inter-quartile range when they are not normally distributed. Categorical values are presented as absolute value and percentage.

Two types of analysis were performed: a patient-level and a frame-level analysis. In patient-level analysis, ANOVA and the Kruskal-Willis test – depending on the distribution of variables – were used for independent group comparison of continuous variables. Comparison between categorical variables was performed using the chi-square test.

In frame-level analysis (to control for the patient effect), a mixed model with random intercept was used to examine the association between stent type and neoatherosclerotic characteristics. A p-value <0.05 was considered statistically significant. Analysis was performed with the SPSS, Version 20 (IBM Corp., Armonk, NY, USA) and the open-source R, version 3.3.0 (The R Foundation for Statistical Computing, Vienna, Austria) statistical packages.

Results

PATIENT CHARACTERISTICS

From November 2009 to September 2015, 41 patients were identified who were deemed suitable for inclusion in the study. After reviewing the data, six patients were excluded, one because of extensive overlapping, one because of no significant in-stent restenosis, three because it was not possible to delineate the stent border in a segment with a length >0.8 mm and one because there was no information about the implanted stent. Therefore, 35 patients (35 stented segments, 11 implanted with a BMS, 13 with a first-generation and 11 with a second-generation DES) were included in the analysis.

As shown in **Table 1**, the three groups had similar baseline characteristics and were receiving similar treatment before being admitted with a cardiovascular event. The only differences noted were in the time interval between index procedure and cardiovascular event, which was increased in the BMS group, and in the stent length which was increased in patients treated with a second-generation DES.

OPTICAL COHERENCE TOMOGRAPHIC ANALYSIS

The total number of analysed frames was 2,304 (568 frames in 11 patients treated with BMS, 860 frames in 13 patients implanted with a first-generation DES and 876 in 11 patients treated with a second-generation DES).

There were no significant differences between groups with regard to the lumen, stent, neointima areas and burden **(Table 2)**. Lipid-rich neoatherosclerotic lesions were identified in 31 patients (10 implanted with a BMS, 12 with a first-generation DES and nine with a second-generation DES), while calcific neoatherosclerotic lesions were detected in 19 patients (six implanted with a BMS, seven with a first-generation and six with a second-generation DES). Lipid-rich and calcific neoatherosclerotic lesions co-existed in 15 patients (six implanted with a BMS, six with a first-generation DES and three with a second-generation DES).

Neoatherosclerotic lesions were the culprit lesions in 31 patients (nine implanted with BMS, 12 with a first- and 10 with a second-generation DES). In the other four cases, stent failure was attributed to restenosis because of excessive neointima proliferation (three cases) and edge restenosis in the distal edge of one stent. As shown in **Figure 1**, neoatherosclerosis had focal manifestations in all stent types. There were no significant differences between different stent types in the number of lipid-rich and calcific neoatherosclerotic lesions, in their length, and in the lipid and calcific areas in these lesions **(Table 2)**. The minimum thickness of the fibrous cap was smaller, and the number of TCFA was increased in BMS (10 in BMS, six in first-generation and five in second-generation DES; p=0.174), but these differences were not statistically significant.

Frame-level analysis demonstrated no significant differences in neointima burden among BMS, first- and second-generation DES **(Table 3)**. Increased thrombus formation and neointima discontinuities were identified in patients implanted with a first-generation DES, while the prevalence of neoatherosclerosis was numerically higher in the BMS group compared to the DES groups, a fact that should be attributed to the numerically higher incidence of lipid-rich neointima. The fibrous cap was thinner and macrophage accumulation was increased in BMS.

Table 1. Baseline characteristics of the studied population.

		BMS (n=11)	First-generation DES (n=13)	Second-generation DES (n=11)	*p*-value
Baseline characteristics	Age (years)	60.1±8.5	61.9±8.0	62.7±9.1	0.751
	Time interval (years)	12.2±2.9	7.8±2.9	2.5±2.7	<0.001
	Male	10 (90%)	10 (76%)	6 (54%)	0.144
	Hypertension	8 (72%)	10 (76%)	7 (63%)	0.768
	Diabetes mellitus	3 (27%)	3 (23%)	5 (45%)	0.469
	Dyslipidaemia	10 (90%)	9 (69%)	7 (63%)	0.298
	Smoking	8 (72%)	5 (38%)	8 (72%)	0.135
	Prior MI	8 (72%)	6 (46%)	5 (45%)	0.333
	Number of diseased vessels	2 (1-3)	1 (1-2)	2 (1-2)	0.323
Clinical presentation at the time of the event	Stable angina	2 (18%)	4 (30%)	2 (18%)	0.718
	NSTEMI*	6 (54%)	7 (53%)	8 (72%)	
	STEMI*	3 (27%)	2 (15%)	1 (9%)	
Medications at the time of the event	Antiplatelet agents*	10 (91%)	10 (83%)	10 (91%)	0.807
	Statins	10 (91%)	9 (75%)	7 (78%)	0.591
	Beta-blockers	7 (64%)	8 (67%)	4 (44%)	0.555
	RAAS inhibitors*	6 (55%)	6 (50%)	4 (44%)	0.904
Treated vessel	Left main stem	0 (0%)	0 (0%)	2 (18%)	0.080
	Left anterior descending artery	7 (64%)	8 (61%)	5 (45%)	
	Left circumflex	4 (36%)	1 (8%)	3 (27%)	
	Right coronary artery	0 (0%)	4 (31%)	1 (9%)	
Baseline PCI*	Length of stented segment (mm)	22.6±6.4	25.1±11.1	36.8±12.4	0.006
	Diameter of stent (mm)	3.00 (3.00-3.50)	3.00 (2.75-3.50)	3.00 (2.75-3.50)	0.860
	Number of stents	1 (1-1)	1 (1-2)	1 (1-2)	0.023

*Antiplatelet agents include: aspirin, clopidogrel, prasugrel and ticagrelor. NSTEMI: non-ST-elevation myocardial infarction; PCI: percutaneous coronary intervention; RAAS inhibitors: renin-angiotensin-aldosterone system inhibitors; STEMI: ST-elevation myocardial infarction

Table 2. Patient-based comparison of OCT data in the three studied groups.

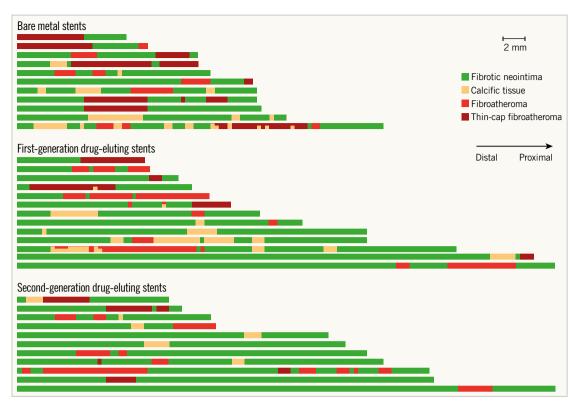|	BMS (n=11)	First-generation DES (n=13)	Second-generation DES (n=11)	*p*-value
Mean lumen area (mm^2)	4.69±1.38	4.64±1.81	4.73±1.93	0.991
Mean stent area (mm^2)	7.22±1.42	7.22±2.25	6.93±2.04	0.921
Mean neointima area (mm^2)	2.54±0.92	2.59±1.30	2.19±1.09	0.665
Neointima burden (%)	36.1 (24.4-45.6)	30.4 (25.4-44.2)	31.1 (19.3-36.6)	0.822
Neoatherosclerotic lesion characteristics				
Number of lipid-rich lesions	2.0 (1.0-2.0)	1.0 (1.0-3.0)	1.0 (1.0-2.0)	0.712
Mean neointima area in lipid-rich lesions (mm^2)	3.04±0.75	3.53±1.19	4.04±1.40	0.181
Mean neointima burden in lipid-rich lesions (%)	41.1 (25.8-46.9)	46.8 (37.7-57.9)	49.3 (26.7-60.4)	0.180
Mean lipid area (mm^2)	1.09±.044	1.34±0.99	1.32±0.47	0.375
Length of lipid-rich lesions (mm)	4.3±2.2	4.9±4.3	4.0±3.7	0.842
Mean lipid angle (degrees)	121.9±33.3	133.4±57.6	149.4±53.7	0.492
Minimum cap thickness (µm)	52±41	96±62	76±46	0.163
Average cap thickness (µm)	189 (172-226)	259 (198-329)	261 (203-291)	0.141
Number of calcific lesions	0 (0-1)	1 (0-1)	1 (0-1)	0.952
Mean neointima area in calcific lesions (mm^2)	3.17±1.35	2.56±1.25	2.54±1.05	0.599
Mean neointima burden in calcific lesions (%)	37.5±12.0	39.9±11.2	37.5±16.7	0.931
Mean calcific area (mm^2)	0.32 (0.25-0.54)	0.42 (0.23-0.45)	0.31 (0.22-0.44)	0.861
Length of calcific lesions (mm)	1.15±1.16	2.12±1.31	2.07±0.59	0.241

Figure 1. *Distribution of neoatherosclerotic lesions in BMS, first- and second-generation DES. Green indicates fibrotic neointima, pink calcific neoatherosclerotic lesions, red fibroatheromas, and dark red TCFA.*

Table 3. Frame-level OCT analysis in the three studied groups.

	BMS (n=11)	First-generation DES (n=13)	Second-generation DES (n=11)	*p*-value
Mean lumen area (mm²)	4.85±1.86	4.25±2.02	4.97±2.54	0.989
Mean stent area (mm²)	7.25±1.65	6.65±2.15	7.16±2.19	0.924
Mean neointima area (mm²)	2.40±1.24	2.41±1.60	2.19±1.55	0.683
Neointima burden (%)	33.83±17.05	35.63±21.10	32.38±21.60	0.914
Neointima characteristics – qualitative analysis				
Frames with neoatherosclerotic lesions	203 (35.7)	216 (25.1)	139 (15.9)	0.089
Frames with lipid-rich neointima	155 (27.3)	155 (18)	113 (12.9)	0.052
Frames portraying TCFA	36 (6.3)	9 (1.0)	12 (1.4)	0.170
Frames portraying calcific-rich neointima	54 (9.5)	66 (7.7)	29 (3.3)	0.550
Frames portraying macrophages	114 (20.1)	89 (10.3)	64 (7.3)	0.012
Frames portraying neo-vessels	5 (0.9)	18 (2.1)	16 (1.8)	0.737
Frames portraying cholesterol crystals	3 (0.5)	11 (1.3)	8 (0.9)	0.657
Frames portraying thrombus	7 (1.2)	88 (10.2)	17 (1.9)	0.032
Frames portraying neointima discontinuities	4 (0.7)	72 (8.4)	4 (0.5)	0.009
Neointima characteristics – qualitative analysis				
Lipid burden (%)	11.3±21.9	6.8±16.4	6.0±16.6	0.362
Lipid angle (degrees)	40.8±77.6	26.2±64.5	24.9±70.2	0.311
Minimum cap thickness (µm)	109±64	189±121	187±0.96	<0.001
Mean cap thickness (µm)	194±81	284±142	303±118	<0.001
Calcific burden (%)	1.7±7.6	1.5±6.0	0.5±3.2	0.701

ATTENUATION AND BACKSCATTER ANALYSIS

Attenuation and backscatter analysis was performed in 30 stented segments (2,074 frames, nine BMS, 12 first-generation and nine second-generation DES). In five cases, processing was not feasible as the data were in DICOM format and the developed algorithm had been designed for the analysis of original raw data. Poor flushing was noted in 101 frames, thrombus in 83, while in 385 frames the region of interest exhibited neointima in an arc <180°. Therefore, 1,505 frames were included in the final analysis **(Figure 2)**.

The attenuation and backscatter indices were increased in BMS compared to DES groups **(Table 4, Figure 3A, Figure 3B)**. Subsegment analysis demonstrated significant differences in attenuation indices between different stent types in neoatherosclerotic lesions but not in the subsegments located adjacent to the neoatherosclerotic lesions or in the subsegments located distally to neoatherosclerotic lesions **(Figure 3C)**. Backscatter indices were also different in subsegments with neoatherosclerotic lesions and in subsegments located distally to neoatherosclerotic lesions, but there were no differences in the subsegments located adjacent to neoatherosclerotic lesions **(Figure 3D)**.
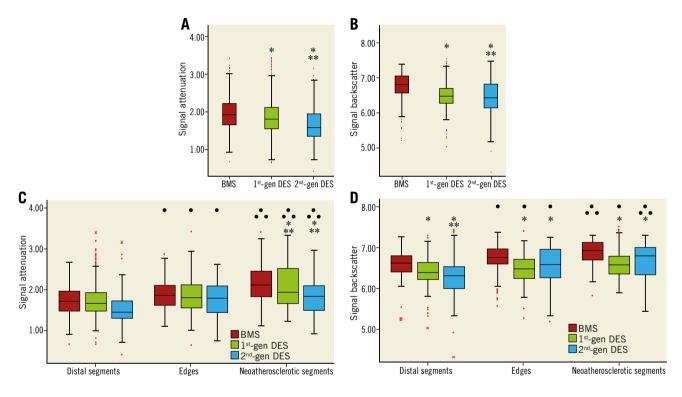
In all stents, the attenuation and backscatter indices increased as we moved from subsegments distal to neoatherosclerotic lesions to subsegments adjacent to these lesions and finally to neoatherosclerotic lesions (p for all three stent types <0.001). When we compared the attenuation and backscatter values among the three subsegments with and without stent type as a random effect (patient was included as a random effect in both models), we found that the effect of stent type was insignificant for both attenuation (p=0.223) and backscatter indices (p=0.090).

Figure 2. *Attenuation and backscatter analysis. Colour-coded display of the attenuation indices in an OCT frame with a neoatherosclerotic lesion, in a frame located adjacent to a neoatherosclerotic lesion, and in a frame distal to a neoatherosclerotic lesion in a patient implanted with a BMS (A-C), first-generation DES (E-G) and second-generation DES (I-K), respectively. Spread-out stent plots of the attenuation indices in a BMS (D), first-generation (H) and second-generation DES (L). The dashed dark green line indicates the location of the frame portraying the neoatherosclerotic lesion (marked with red transparent colour in the spread-out stent plots), the dashed green line the frame obtained from a subsegment adjacent to a neoatherosclerotic lesion (marked with yellow transparent colour in the spread-out stent plots) and the dashed light green line the frame obtained from a subsegment located distally to a neoatherosclerotic lesion (marked with blue transparent colour in the spread-out stent plots).*

Table 4. Attenuation and backscatter indices at the time of the event in patients implanted with a BMS, first-generation and second-generation DES.

	BMS (n=9)	First-generation DES (n=12)	Second-generation DES (n=9)	*p*-value
Attenuation indices				
Mean values	2.30 (1.98-2.72)	2.10 (1.80-2.49)	1.83 (1.57-2.29)	0.031
Neoatherosclerotic segments	2.54 (2.27-3.07)	2.36 (1.96-2.99)	2.20 (1.79-2.53)	0.016
At the edges of neoatherosclerotic segments	2.18 (1.93-2.50)	2.18 (1.83-2.54)	2.08 (1.66-2.40)	0.372
Distally to neoatherosclerotic segments	2.04 (1.68-2.39)	1.96 (1.73-2.26)	1.70 (1.52-1.99)	0.224
Backscatter indices				
Mean values	7.00 (6.78-7.22)	6.66 (6.46-6.89)	6.63 (6.33-7.01)	0.018
Neoatherosclerotic segments	6.96 (6.72-7.17)	6.80 (6.57-7.01)	6.81 (6.37-7.02)	0.033
At the edges of neoatherosclerotic segments	6.96 (6.80-7.18)	6.70 (6.46-6.94)	6.79 (6.47-7.13)	0.083
Distally to neoatherosclerotic segments	6.82 (6.58-7.02)	6.59 (6.42-6.81)	6.48 (6.21-6.72)	0.042

Figure 3. *Box plots of the attenuation and backscatter analysis. Attenuation (A) and backscatter (B) indices in BMS, first-generation DES (1st-gen DES) and second-generation DES (2nd-gen DES).* ✱*Indicates statistically significant differences (p<0.05) between the BMS and the DES groups.* ✱✱*Indicates statistically significant differences between first-generation and second-generation DES. Attenuation (C) and backscatter (D) indices in the subsegments located distally (distal segments), adjacent to neoatherosclerotic subsegments (edges) and in neoatherosclerotic lesions (neoatherosclerotic segments).* ✱*Indicates statistically significant differences in the attenuation/backscatter indices between corresponding BMS and first- or second-generation DES subsegments.* ✱✱*Denotes statistically significant differences between first- and second-generation DES.* ●*Indicates statistically significant differences in the attenuation/backscatter indices between subsegments located distally to neoatherosclerotic lesions and the subsegments adjacent to neoatherosclerotic or at the neoatherosclerotic lesions in each stent type.* ●●*Denotes statistically significant differences between subsegments located adjacent to neoatherosclerotic lesions and the subsegments with neoatherosclerotic lesions.*

Discussion

In this study we examined for the first time the morphological characteristics of the neointima in different stent types in patients with neoatherosclerotic lesions admitted with a cardiovascular event attributed to stent failure. We found: 1) no differences in neointima burden in different stents, but 2) increased lipid tissue burden and macrophage accumulation in BMS at the time of the event, 3) a higher incidence of thrombus and neointima discontinuities

in first-generation DES, 4) increased backscatter and attenuation indices in BMS, and 5) that the attenuation and backscatter indices are higher in neoatherosclerotic lesions in BMS, but 6) the attenuation indices are not different and have low values in subsegments without neoatherosclerotic lesions in all stent types.

Our findings are in agreement with previous reports showing that, compared to DES, BMS failure because of neoatherosclerotic lesion formation occurs later after the index procedure[12]. Short-term follow-up intravascular imaging studies (up to one year) have demonstrated increased neointima hyperplasia in BMS compared to first- and second-generation DES[13]; however, this trend appears to change in the long term as neointima starts to develop in DES after the first year of implantation – resulting in the so-called late catch-up phenomenon – and recent long-term intravascular imaging studies have shown comparable neointima burden at long-term (>1 year) follow-up[14].

Despite the absence of differences in neointima burden, we reported significant differences in neointima morphology between stent types. Neoatherosclerotic burden was numerically higher in the BMS patients, mainly because of an increase in the lipid-rich neointima in this group. In addition, the fibrous cap was thinner and the incidence of macrophage accumulation was higher in BMS compared to DES groups. These differences should be attributed not only to the different pathophysiological mechanisms underlying neoatherosclerotic lesion formation in different stent types[1], but also to the increased time interval between index procedure and cardiovascular events noted in the BMS group that allowed degeneration of the neointima to lipid-rich lesions and their maturation and formation of high-risk vulnerable plaques[4,6].

Despite the fact that the follow-up period was shorter in the first-generation DES compared to BMS, we found an increased frequency of neointima discontinuities and thrombus formation in this stent group. Our results are in agreement with a recent report that demonstrated an increased incidence of thrombus burden in first-generation compared to second-generation DES[3]. A possible explanation of this finding is the focal inflammation noted in this stent group that is triggered by a hypersensitivity reaction to the polymer. This process appears to result in eosinophil infiltration[15], strut malapposition and, finally, stent thrombosis; however, it is also likely to promote the early formation of unstable neoatherosclerotic lesions and their destabilisation, resulting in extensive rupture[1]. The modification of stent design in the second-generation DES and, in particular, the reduction of the diameter of stent struts, the use of biocompatible polymers and different drug elutions[16], as well as the difference in time interval between device implantation and cardiovascular event in our study may account for the low incidence of neoatherosclerosis in this group.

Histology-based studies have shown increased attenuation and backscatter indices in lipid-rich plaques and in lesions rich in macrophages. Methodologies have been developed that take into account this information to characterise plaque morphology. In this study, we developed a module that enables quantification of these indices in order to assess degenerative changes in neointima in different stent types. We found higher attenuation and backscatter indices in BMS compared to DES: this should be attributed to the increased lipid-rich neointima and macrophage accumulation noted in this group. More interestingly, we found low and not statistically different attenuation indices in subsegments located distally and adjacent to neoatherosclerotic lesions in all stent types. This finding indicates that neoatherosclerosis, similar to atherosclerosis, has focal manifestations, suggesting that, apart from systemic factors such as high-risk vulnerable patients[17], endothelial dysfunction or an inflammatory reaction to the drug or the polymer[1], other focal factors are also likely to contribute to the formation of vulnerable lesions. Indeed, a histology study recently demonstrated that the presence of underlying high-risk plaques predicts neoatherosclerotic lesion formation[18]. In our study, in 60% of the calcific neoatherosclerotic lesions the calcific tissue extended in the underlying plaque. There is speculation that the local haemodynamic forces may also contribute to neoatherosclerotic lesion formation[1]; however, there is no robust evidence to support this hypothesis. Future studies that will use advanced imaging techniques are expected to allow us to investigate the role of the local haemodynamic forces, of plaque strain following stent implantation, and of the local inflammation[19] on neoatherosclerotic lesion formation, and reshape our treatment strategies (i.e., either by designing advanced stent platforms that will have a minimal effect on the local haemodynamic forces and minimise vessel wall trauma or by administering pharmacotherapy that will target the underlying inflamed plaques) so as to reduce the incidence of neoatherosclerosis and improve clinical outcomes.

Limitations

There are several limitations in this study. First, the small number of patients included may have significantly affected the power of the statistical analysis and did not allow us to investigate the effect of the time difference between index procedure and cardiovascular event on the neoatherosclerotic characteristics in different stent groups. Secondly, this was a retrospective analysis and therefore, although we included consecutive patients, it is likely that changes in clinical practice such as the move from BMS to first-generation and then to second-generation DES implantation might have introduced bias with regard to the time interval between index procedure and cardiovascular events in different stent groups. Moreover, in order to perform a detailed qualitative and quantitative analysis of neointima morphology, we excluded segments with extensive thrombus or lipid burden that did not allow visualisation of stent circumference in the entire stent. This may have introduced bias but, nevertheless, it is reassuring that our findings are in agreement with other published reports[2-4]. Finally, it should be acknowledged that in this study there was no control group that would have allowed us to compare plaque characteristics in symptomatic and asymptomatic patients, and the baseline OCT data before or after stent implantation were lacking; therefore, it was not possible to evaluate the role of the underlying plaque on neoatherosclerotic evolution.

Conclusions

We found a significant variation in the phenotypic characteristics of the neointima in different stent types in patients with neoatherosclerotic lesions admitted with a cardiovascular event attributed to stent failure. In BMS, neoatherosclerotic lesions had a more vulnerable morphology with a numerically increased lipid-rich neointima, thinner fibrous caps and a higher incidence of macrophage accumulation, whereas in first-generation DES there was an increased incidence of neointima discontinuities and thrombus burden. In all stent types, however, neoatherosclerosis had focal manifestations, a finding that suggests that, apart from systemic or stent-related factors, local triggers are also involved in the formation of vulnerable neolesions.

Impact on daily practice

Despite the fact that neoatherosclerosis has different morphological characteristics in BMS, first- and second-generation DES in patients admitted with stent failure, in all stent types it has focal manifestations, indicating that local triggers also contribute to the generation of vulnerable neolesions. Understanding the focal mechanisms regulating their formation is crucial in order to reduce the incidence of neoatherosclerosis and improve clinical outcomes.

Guest Editor

This paper was guest edited by Peter Barlis, MBBS, MPH, PhD; Melbourne Medical School, University of Melbourne, Melbourne, Victoria, Australia.

Funding

Conflict of interest statement

The authors have no conflicts of interest to declare. The Guest Editor has no conflicts of interest to declare.

References

1. Otsuka F, Byrne RA, Yahagi K, Mori H, Ladich E, Fowler DR, Kutys R, Xhepa E, Kastrati A, Virmani R, Joner M. Neoatherosclerosis: overview of histopathologic findings and implications for intravascular imaging assessment. *Eur Heart J.* 2015;36:2147-59.

2. Nakamura D, Attizzani GF, Toma C, Sheth T, Wang W, Soud M, Aoun R, Tummala R, Leygerman M, Fares A, Mehanna E, Nishino S, Fung A, Costa MA, Bezerra HG. Failure Mechanisms and Neoatherosclerosis Patterns in Very Late Drug-Eluting and Bare-Metal Stent Thrombosis. *Circ Cardiovasc Interv.* 2016 Sep;9(9).

3. Song L, Mintz GS, Yin D, Yamamoto MH, Chin CY, Matsumura M, Fall K, Kirtane AJ, Parikh MA, Moses JW, Ali ZA, Shlofmitz RA, Maehara A. Neoatherosclerosis assessed with optical coherence tomography in restenotic bare metal and first- and second-generation drug-eluting stents. *Int J Cardiovasc Imaging.* 2017;33:1115-24.

4. Yonetsu T, Kim JS, Kato K, Kim SJ, Xing L, Yeh RW, Sakhuja R, McNulty I, Lee H, Zhang S, Uemura S, Yu B, Kakuta T, Jang IK. Comparison of incidence and time course of neoatherosclerosis between bare metal stents and drug-eluting stents using optical coherence tomography. *Am J Cardiol.* 2012;110:933-9.

5. Gao L, Park SJ, Jang Y, Lee S, Kim CJ, Minami Y, Ong D, Soeda T, Vergallo R, Lee H, Yu B, Uemura S, Jang IK. Comparison of Neoatherosclerosis and Neovascularization Between Patients With and Without Diabetes: An Optical Coherence Tomography Study. *JACC Cardiovasc Interv.* 2015;8:1044-52.

6. Yonetsu T, Kato K, Kim SJ, Xing L, Jia H, McNulty I, Lee H, Zhang S, Uemura S, Jang Y, Kang SJ, Park SJ, Lee S, Yu B, Kakuta T, Jang IK. Predictors for neoatherosclerosis: a retrospective observational study from the optical coherence tomography registry. *Circ Cardiovasc Imaging.* 2012;5:660-6.

7. Tearney GJ, Regar E, Akasaka T, Adriaenssens T, Barlis P, Bezerra HG, Bouma B, Bruining N, Cho JM, Chowdhary S, Costa MA, de Silva R, Dijkstra J, Di Mario C, Dudek D, Falk E, Feldman MD, Fitzgerald P, Garcia-Garcia HM, Gonzalo N, Granada JF, Guagliumi G, Holm NR, Honda Y, Ikeno F, Kawasaki M, Kochman J, Koltowski L, Kubo T, Kume T, Kyono H, Lam CC, Lamouche G, Lee DP, Leon MB, Maehara A, Manfrini O, Mintz GS, Mizuno K, Morel MA, Nadkarni S, Okura H, Otake H, Pietrasik A, Prati F, Raber L, Radu MD, Rieber J, Riga M, Rollins A, Rosenberg M, Sirbu V, Serruys PW, Shimada K, Shinke T, Shite J, Siegel E, Sonoda S, Suter M, Takarada S, Tanaka A, Terashima M, Thim T, Uemura S, Ughi GJ, van Beusekom HM, van der Steen AF, van Es GA, van Soest G, Virmani R, Waxman S, Weissman NJ, Weisz G; International Working Group for Intravascular Optical Coherence Tomography (IWG-IVOCT). Consensus standards for acquisition, measurement, and reporting of intravascular optical coherence tomography studies: a report from the International Working Group for Intravascular Optical Coherence Tomography Standardization and Validation. *J Am Coll Cardiol.* 2012;59:1058-72.

8. Radu MD, Yamaji K, Garcia-Garcia HM, Zaugg S, Taniwaki M, Koskinas KC, Serruys PW, Windecker S, Dijkstra J, Raber L. Variability in the measurement of minimum fibrous cap thickness and reproducibility of fibroatheroma classification by optical coherence tomography using manual versus semi-automatic assessment. *EuroIntervention.* 2016;12:e987-97.

9. Bourantas CV, Serruys PW, Nakatani S, Zhang YJ, Farooq V, Diletti R, Ligthart J, Sheehy A, van Geuns RJ, McClean D, Chevalier B, Windecker S, Koolen J, Ormiston J, Whitbourn R, Rapoza R, Veldhof S, Onuma Y, Garcia-Garcia HM. Bioresorbable vascular scaffold treatment induces the formation of neointimal cap that seals the underlying plaque without compromising the luminal dimensions: a concept based on serial optical coherence tomography data. *EuroIntervention.* 2015;11:746-56.

10. Vermeer KA, Mo J, Weda JJ, Lemij HG, de Boer JF. Depth-resolved model-based reconstruction of attenuation coefficients in optical coherence tomography. *Biomed Opt Express.* 2013;5: 322-37.

11. Schmitt JM, Knuttel A, Bonner RF. Measurement of optical properties of biological tissues by low-coherence reflectometry. *Appl Opt.* 1993;32:6032-42.

12. Souteyrand G, Amabile N, Mangin L, Chabin X, Meneveau N, Cayla G, Vanzetto G, Barnay P, Trouillet C, Rioufol G, Range G, Teiger E, Delaunay R, Dubreuil O, Lhermusier T, Mulliez A, Levesque S, Belle L, Caussin C, Motreff P; PESTO Investigators. Mechanisms of stent thrombosis analysed by optical coherence tomography: insights from the national PESTO French registry. *Eur Heart J.* 2016;37:1208-16.

13. Iannaccone M, D'Ascenzo F, Templin C, Omedè P, Montefusco A, Guagliumi G, Serruys PW, Di Mario C, Kochman J, Quadri G, Biondi-Zoccai G, Luscher TF, Moretti C, D'Amico M, Gaita F, Stone GW. Optical coherence tomography evaluation of intermediate-term healing of different stent types: systemic review and meta-analysis. *Eur Heart J Cardiovasc Imaging.* 2017;18: 159-66.

14. Goto K, Zhao Z, Matsumura M, Dohi T, Kobayashi N, Kirtane AJ, Rabbani LE, Collins MB, Parikh MA, Kodali SK, Leon MB, Moses JW, Mintz GS, Maehara A. Mechanisms and Patterns of Intravascular Ultrasound In-Stent Restenosis Among Bare Metal Stents and First- and Second-Generation Drug-Eluting Stents. *Am J Cardiol.* 2015;116:1351-7.

15. Cook S, Ladich E, Nakazawa G, Eshtehardi P, Neidhart M, Vogel R, Togni M, Wenaweser P, Billinger M, Seiler C, Gay S, Meier B, Pichler WJ, Juni P, Virmani R, Windecker S. Correlation of intravascular ultrasound findings with histopathological analysis of thrombus aspirates in patients with very late drug-eluting stent thrombosis. *Circulation.* 2009;120:391-9.

16. Steigerwald K, Ballke S, Quee SC, Byrne RA, Vorpahl M, Vogeser M, Kolodgie F, Virmani R, Joner M. Vascular healing in drug-eluting stents: differential drug-associated response of limus-eluting stents in a preclinical model of stent implantation. *EuroIntervention.* 2012;8:752-9.

17. Taniwaki M, Windecker S, Zaugg S, Stefanini GG, Baumgartner S, Zanchin T, Wenaweser P, Meier B, Jüni P, Räber L. The association between in-stent neoatherosclerosis and native coronary artery disease progression: a long-term angiographic and optical coherence tomography cohort study. *Eur Heart J.* 2015;36:2167-76.

18. Nakazawa G, Otsuka F, Nakano M, Vorpahl M, Yazdani SK, Ladich E, Kolodgie FD, Finn AV, Virmani R. The pathology of neo-atherosclerosis in human coronary implants bare-metal and drug-eluting stents. *J Am Coll Cardiol.* 2011;57:1314-22.

19. Kim S, Lee MW, Kim TS, Song JW, Nam HS, Cho HS, Jang SJ, Ryu J, Oh DJ, Gweon DG, Park SH, Park K, Oh WY, Yoo H, Kim JW. Intracoronary dual-modal optical coherence tomography-near-infrared fluorescence structural-molecular imaging with a clinical dose of indocyanine green for the assessment of high-risk plaques and stent-associated inflammation in a beating coronary artery. *Eur Heart J.* 2016;37:2833-44.